Positron states at a lithium-adsorbed Al(100) surface: Two-component density functional theory simulation

Satoshi Hagiwara, Chunping Hu, and Kazuyuki Watanabe*
Department of Physics, Tokyo University of Science, 1-3 Kagurazaka, Shinjuku-ku, Tokyo 162-8601, Japan
(Received 17 November 2014; revised manuscript received 15 January 2015; published 6 March 2015)

The positron surface state and the energetics for positron reemission are investigated using two-component density functional theory (TC-DFT) in the projector augmented-wave framework. Trapping of positrons by the surface image potential and the effect of the positron band-shift energy in the surface region are appropriately described by the corrugated mirror model and the ramp potential, respectively, without empirical parameters. The results obtained for various physical quantities of positron states on a clean Al(100) surface, i.e., the affinity, work function, life-time, binding energy, and activation energy, are in good agreement with the experimental results. The positron states on Li-adsorbed Al(100) surfaces are highly dependent on the Li coverage. In particular, the work function of positronium negative ions (Ps^-) becomes negative at low Li coverage, which indicates the possible emission of Ps^- from the adsorbed surface. The present study not only elucidates the key energetics that are responsible for positron reemission from the surface, but also emphasizes the excellent performance of TC-DFT for prediction of the positron state on real surfaces.

DOI: 10.1103/PhysRevB.91.115409 PACS number(s): 71.60.+z, 31.15.E−, 68.43.−h, 78.70.Bj

I. INTRODUCTION

Positron annihilation spectroscopy [1–3] has attracted much attention because positrons are a very sensitive probe and a powerful tool for the analysis of vacancy-type defects in crystals. A positron annihilates with an electron in a crystal to produce γ-rays, which provides information on the electronic states in crystals with and without vacancy defects. For the study of surface physics, a slow positron beam is a powerful tool in reemitted positron energy loss spectroscopy [4], positron-annihilation-induced Auger electron spectroscopy [5,6], and reflection high-energy positron diffraction [7]. Furthermore, experimental methods using positronium (Ps), which is a bound state of an electron and a positron, have also been developed for surface studies. Michishio *et al.* [8] have succeeded in producing an energy-tunable monoenergy Ps beam. The Ps beam is produced from the positronium negative ion (Ps^-) [9], which is a bound state of a single positron and two electrons, using the photodetachment technique [10]. The Ps beam has a neutral charge and is thus expected to be a promising tool for the study of insulator surfaces.

One of the most important properties of positrons at surfaces is the negative work function for many metal surfaces, by which a positron that is slowly injected into a metal surface can be spontaneously reemitted to the vacuum through thermal diffusion from inside the bulk to the surface. When the positron returns to the surface region, the positron may be combined with one or two electrons and emitted as a Ps or Ps^-. Whether these processes occur can be evaluated from the values of the Ps and Ps^- work functions for that surface. If the Ps^- can be steadily formed in such a way to produce a large amount of Ps^-, a Ps beam can be produced with stronger intensity, which can be used to significantly advance the study of surface physics. On the other hand, a positron can also be trapped in the surface region by the surface image potential [11,12] and then annihilate or become a thermalized Ps atom with a surface electron. Therefore, determination of the work function and surface-trapped states of positrons is required to understand the positron reemission process.

Theoretical investigations on the surface states of positrons are not yet complete, particularly with the first-principles calculation methods. Puska and Nieminen [3,13] have developed a flexible superimposed-atom method for the study of positrons under various conditions. The electron density is constructed simply by superimposing free atoms in the appropriate geometry. This technique has been shown to produce reliable results for many practical applications [14–18]. On the other hand, studies on the positron states in the bulk crystal using the self-consistent electron densities of optimized atomic geometries have been conducted using two-component density functional theory (TC-DFT) [1,19–28], which is known to well reproduce the experimentally measured positron lifetimes, both in perfect crystals and crystals with vacancy defects [29–37]. However, for the surface, the TC-DFT scheme has only been applied to the study of positrons at jellium substrates that have neither realistic atomic configurations nor variation of electron density near atoms [38–40].

In the present study, we aim to understand the basics of positron states at metal surfaces using first-principles TC-DFT simulations of surfaces *with realistic atomic configurations.* The self-consistent electron density of the fully relaxed atomic geometry is used as the input for calculation of the positron states. The corrugated mirror model (CMM) is used together with the ramp potential without any empirical parameters by taking account of the surface image potential and the band-shift energy. This scheme is applied to Al(100) surfaces with various Li-coverage. Good agreement with the previous results on positron work functions and the positron surface-state properties has been obtained for the well-studied clean surface. For the Li-adsorbed surfaces that have not been previously studied, the work functions of Ps^- become negative at low Li coverage, which indicates possible emission of Ps^- from such surfaces.

*kazuyuki@rs.kagu.tus.ac.jp

The present paper is organized as follows. In Sec. II the basic formalism of TC-DFT, a discussion on the CMM model and the ramp potential, and the scheme for the positron surface-state lifetime are described. The slab model and computational details on electron and positron states are given in Sec. III. In Sec. IV results are presented for the positron affinity, work functions of electrons, positrons, Ps, and Ps^-, as well as the positron surface-state lifetime, binding energies, and activation energies for Al(100) surfaces. Conclusions are given in Sec. V.

II. METHODS

A. Two-component density functional theory

In the present study, we perform calculations of positron states for the Al bulk and surfaces based on the TC-DFT conventional scheme [1,20,27,41]. First, the electron Kohn-Sham (KS) equation is solved by the ordinary DFT scheme without the positron and the self-consistent electronic structure of the relaxed atomic geometry is obtained. Then, the positron equation is solved with the input of the calculated electron ground-state density, n_-, to obtain the positron ground state. The KS equation for positron is expressed as (atomic units are used throughout this section, unless stated otherwise)

$$\left[-\frac{\nabla^2}{2}+\frac{\delta E_{\rm xc}[n_+]}{\delta n_+}+\phi(\mathbf{r})+\frac{\delta E_{\rm corr}^{e-p}[n_+]}{\delta n_+}\right]\psi_j^+(\mathbf{r})=E_j^+\psi_j^+(\mathbf{r}), \tag{1}$$

where

$$\phi(\mathbf{r})=\int d\mathbf{r}'\frac{-n_-(\mathbf{r}')+n_+(\mathbf{r}')+n_0(\mathbf{r}')}{|\mathbf{r}-\mathbf{r}'|}. \tag{2}$$

Here, $E_{\rm xc}[n_+]$ is exchange-correlation energy for positrons, ψ_j^+ and E_j^+ are KS orbitals and eigenenergies for positrons, and $\phi(\mathbf{r})$ and $n_0(\mathbf{r})$ are the electrostatic potential and ion core density, respectively. We assume a single positron in the calculation box, so that the self-interaction term in the positron KS equation is removed, and the equation becomes

$$\left[-\frac{\nabla^2}{2}+\phi'(\mathbf{r})+\frac{\delta E_{\rm corr}^{e-p}[n_+]}{\delta n_+}\right]\psi_j^+(\mathbf{r})=E^+\psi_j^+(\mathbf{r}), \tag{3}$$

with

$$\phi'(\mathbf{r})=\int d\mathbf{r}'\frac{-n_-(\mathbf{r}')+n_0(\mathbf{r}')}{|\mathbf{r}-\mathbf{r}'|}. \tag{4}$$

The positron bulk- and surface-state properties can then be calculated from the electron and positron density distributions.

B. Positron surface potential

Thermalized positrons near a surface are considered to be trapped by the surface image potential. To study the state of a surface-trapped positron, a slab model is used to represent the metal surface, as in typical DFT calculations. However, simulation of the positron surface state in the slab model has two problems. One is the description of the electron-positron correlation potential in the vacuum region and the other is that of the positron effective potential in the slab region [38,40]. The electron-positron correlation potential can be well described in the bulk crystal with or without vacancy defects using ordinary density functionals such as those based on the local density approximation (LDA) and the generalized gradient approximation (GGA). However, the correlation potential in the slab model within the LDA or GGA does not include the effect of the surface image potential, and thus the positron surface state cannot be correctly calculated. To overcome this problem, the so-called corrugated mirror model (CMM) [42] is adopted to correct the positron surface potential. In this model, the image potential has the same corrugations as the electron density, and the image potential in the CMM is expressed by

$$V_{\rm corr}(z\to\infty)=-\frac{1}{4(z-z_0)},\quad z_0<z. \tag{5}$$

Here, the z axis is perpendicular to the surface and z_0 is the position of the effective image plane, which corresponds to the center of mass of surface charge distributions. The value of z_0 is determined using the method reported by Lang and Kohn [43]. It is noted that Eq. (5) has an unphysical divergence near the $z=z_0$ region. To remove this divergence, a cutoff energy of 6.8 eV is used, which corresponds to the binding energy of Ps, for the magnitude of the image potential [42]. The image potential is smoothly connected to the electron-positron correlation potential in the bulk region of the slab.

The other problem in the description of the positron effective potential in the slab calculation is related to the positron band-shift energy, which is the positron zero-point energy arising from the positron-ion interaction [44]. The band-shift energy is a constant (E_0) in the bulk and is damped to zero in the vacuum. To take account of this effect, the positron effective potential is added as a compensation potential in the form of the ramp potential as [14–18]

$$V_{\rm ramp}(z)=\begin{cases}E_0, & z<z_1,\\ E_0(z-z_2)/(z_1-z_2), & z_1<z<z_2,\\ 0, & z_2<z.\end{cases} \tag{6}$$

where z_1 is the atomic position in the topmost surface layer (in Fig. 1) and z_2 is the position distant from z_1 to the vacuum by a half of the interlayer distance of the bulk. z_2 is regarded as the physical edge position of the metal surface in the jellium model [43]. E_0 is given by [45]

$$\begin{aligned}E_0&=-(-\Phi_+ + |D+E_{\rm corr}|)\\ &=\Phi_+-|D+E_{\rm corr}|,\end{aligned} \tag{7}$$

where Φ_+ is the positron work function, D is the surface dipole barrier, $E_{\rm corr}$ is the positron-electron correlation energy, and $|D+E_{\rm corr}|$ is the energy of the bottom of the positron effective potential with respect to the vacuum level. A schematic illustration of these potentials is shown in Fig. 1. The TC-DFT calculation for a positron in the bulk crystal is conducted first and the positron affinity A_+ is obtained from the electron (positron) chemical potential, μ_- (μ_+) as [46,47]

$$A_+=\mu_-+\mu_+. \tag{8}$$

The electron work function Φ_-, which is obtained in the DFT calculation of the slab, is then used to determine the positron work function as

$$\Phi_+=-D-\mu_+=-(\Phi_-+\mu_-)-\mu_+=-A_+-\Phi_-. \tag{9}$$

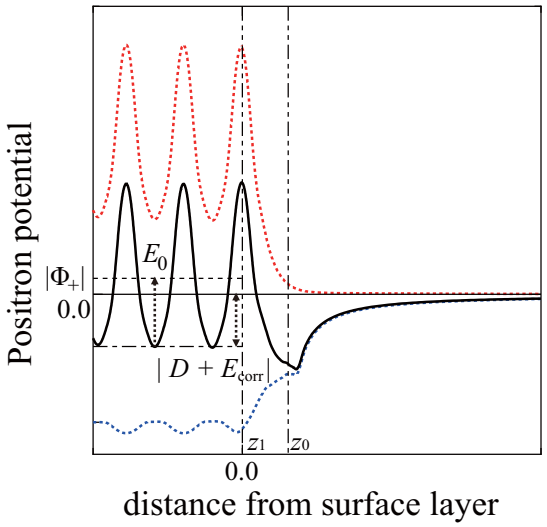

FIG. 1. (Color online) Schematic of the potentials for a positron at a clean metal surface. The solid black curve represents the effective potential for the positron, and the red and blue dotted curves represent the electrostatic and electron-positron correlation potential, respectively. The positron work function is denoted as Φ_+, which has a negative value. The band-shift energy measured from the bottom of the effective potential is denoted by E_0. Coordinates z_1 and z_0 denote the positions of the topmost surface layer and the effective image plane, respectively.

E_0 [in Eq. (7)] is thus determined by first-principles calculations. For comparison, the compensation potential is obtained by resorting to the experimental positron work function in the previous studies of superimposed-atom methods [14–18].

C. The positron lifetime

The positron lifetime τ, is dependent on both the positron and electron ground-state densities, $n_+(\mathbf{r})$ and $n_-(\mathbf{r})$, and is calculated from the inverse of the annihilation rate λ as

$$\frac{1}{\tau} = \lambda = \pi c r_0^2 \int d\mathbf{r} n_-(\mathbf{r}) n_+(\mathbf{r}) \gamma(n_-), \tag{10}$$

where c is the velocity of light and r_0 is the classical electron radius. $\gamma(n_-)$ is an enhancement factor caused by the electron-positron correlation effect that takes account of an increase in the electron density at the positron site due to screening of the positron by electrons. $\gamma(n_-)$ is set to zero in the image potential region ($z > z_0$ in Fig. 1), where the electron screening effect is negligible [48].

III. MODEL AND COMPUTATIONAL DETAILS

In this study, TC-DFT calculations were conducted for the positron surface state at the Al(100) surface with Li adatoms. The surface is represented by a slab having seven atomic layers and a vacuum region with a thickness of 40 Å. The atomic geometry in the slab is optimized and all calculations of the electron and positron states are performed using the free-source program package ABINIT [49,50] within the projector augmented-wave (PAW) [51,52] method.

A. Computational details for the electronic states

The PAW potentials were generated using the all-electron calculation code ATOMPAW [53]. For the Al and Li atoms, the valence electron configurations were $2s^2 2p^6 3s^2 3p^1$ and $1s^2 2s^1$, respectively. The number of $\mathbf{k}$ point sampling was $10 \times 10 \times 10$ for the Al bulk (perfect crystal) calculation and $10 \times 10 \times 1$ for the slab calculations. The kinetic energy cutoff was 20 Ha for Al bulk and the clean Al surface, and 25 Ha for the Al surface with Li adatoms. The GGA functional parameterized by Perdew, Burke, and Ernzerhof (PBE) [54] was used. Cell optimization was performed for the Al bulk and the theoretical lattice constant was obtained as 4.04 Å, which was used for construction of the slab. The atomic geometry in the slab was then relaxed along the direction perpendicular to the surface until all the forces acting on the Al atoms were smaller than 5.0×10^{-4} Ha/bohr. The adsorption sites of Li atoms on the Al(100) surface were chosen as hollow sites and the adsorption distances were optimized for different Li coverage.

B. Computational details for the positron states

The CMM and ramp potential were implemented into the ABINIT code for the positron calculation. The same cutoff energy was used as that for the electronic ground-state calculations. Only the Γ point ($\mathbf{k} = \mathbf{0}$) was used in the $\mathbf{k}$-point sampling. For a comparative study on the dependence of the electron-positron correlation energy functionals, the LDA functionals with two different parametrization schemes were used: the Boroński and Nieminen (BN) [20] scheme as a parametrization of the data from Arponen and Pajanne (AP) [55], and the Sterne and Kaiser (SK) [56] scheme based on the AP result. The BN and SK schemes were also used with the GGA correction [57–59]. These functionals have different forms for the correlation potential and enhancement factor.

IV. RESULTS AND DISCUSSIONS

In this section, we present the simulation results for a positron at an Al(100) surface with Li adatoms using TC-DFT calculations. We first show the results for the electron and positron work functions with various Li coverage before discussing the results for the positron surface-state properties that are responsible for positron reemission.

A. Work functions for electron and positron

First, we present the results for the positron, Ps, and Ps^- work functions, which are calculated from the positron affinity (A_+) and electron work function. Table I shows the A_+ results

TABLE I. Positron affinities (A_+) calculated with the BN and SK schemes for the LDA and GGA and that reported for an experiment (in eV).

LDA		GGA		
A_+^{BN}	A_+^{SK}	A_+^{BN}	A_+^{SK}	A_+^{exp}
−4.34	−4.33	−4.11	−4.14	−4.2[a]

[a]Ref. [60].

TABLE II. Work functions of electrons (Φ_-) and positrons (Φ_+) for the Al(100) surface with various Li coverage, calculated with the BN and SK schemes for LDA and GGA and that reported for experiments (in eV).

		LDA		GGA			
	Φ_-	Φ_+^{BN}	Φ_+^{SK}	Φ_+^{BN}	Φ_+^{SK}	Φ_-^{exp}	Φ_+^{exp}
Clean	4.39	−0.046	−0.061	−0.267	−0.287	4.41[a]	−0.19[b]
Li adsorbed							
0.25 ML	2.18	2.15	2.14	1.93	1.91	–	–
0.50 ML	2.47	1.87	1.85	1.65	1.63	–	–
0.75 ML	2.93	1.41	1.40	1.19	1.17	–	–
1.00 ML	3.33	1.01	0.997	0.792	0.771	–	–

[a]Ref. [63].
[b]Ref. [64].

from the calculation of a positron in the Al bulk. The BN and SK schemes give similar results and both the LDA and GGA well reproduce the experimental value. A lower A_+ in the LDA than in the GGA was obtained in the previous theoretical studies [57,59].

Table II shows the results for the electron and positron work functions, Φ_- and Φ_+, for Al(100) surfaces with various Li coverage. Φ_- was calculated as the difference between the vacuum level and the Fermi energy of electrons, while Φ_+ was calculated from Eq. (9). Φ_- and Φ_+ calculated for the clean Al(100) surface are in good agreement with the experimental data. For the Al surfaces with Li adatoms, both Φ_- and Φ_+ are strongly dependent on the Li coverage, but with opposite tendencies. Φ_- (Φ_+) abruptly decreases (increases) at 0.25 monolayer (ML) coverage and then increases (decreases) with increasing coverage until 1.00 ML. The BN and SK schemes give similar results for all Li coverage examined. There is a tendency that the LDA gives a higher Φ_+ than GGA, which is opposite to that for A_+ in Table I (note that $-A_+$ contributes to Φ_+). With respect to the physical origin for the change in Φ_-, it is well known in surface physics that the initial drastic decrease in Φ_- is due to electronic charge transfer from the Li adatom to the Al substrate because the electron affinity of lithium is smaller than that of aluminum, which results in a reduction of the surface dipole barrier that prevents electrons from escaping into the vacuum. At higher Li coverage, however, bonding between the lone 2*s* electrons of Li atoms can occur and this suppresses electron transfer from Li atoms to the Al substrate. The dependence of Φ_+ on the Li coverage can also be understood in this way and is consistent with the experimental results for other metal surfaces with different species of adsorbed atoms [61,62]. It is noted that Φ_+ becomes positive at finite Li coverage, which means that positrons are easily trapped inside an Al(100) surface covered with Li adatoms.

Table III shows the Ps work functions, Φ_{Ps}, for the Al(100) surface calculated using

$$\Phi_{Ps} = \Phi_- + \Phi_+ - E_b^{Ps} = -A_+ - E_b^{Ps}, \qquad (11)$$

where $E_b^{Ps} = 6.8$ eV, which is the binding energy of Ps. It is noted that Φ_{Ps} is not affected by the change of the surface dipole barrier, because the effects of the surface dipole on

TABLE III. Ps work function (Φ_{Ps}) for the clean Al(100) surface, calculated with the BN and SK schemes for LDA and GGA and that reported for an experiment (in eV).

LDA		GGA		
Φ_{Ps}^{BN}	Φ_{Ps}^{SK}	Φ_{Ps}^{BN}	Φ_{Ps}^{SK}	Φ_{Ps}^{exp}
−2.45	−2.46	−2.67	−2.69	−2.6[a]

[a]Ref. [60].

Φ_{Ps} for electrons and positrons become canceled for Ps, as in Eq. (11). Therefore, the Ps work function shows no dependence on the Li coverage. The calculated Φ_{Ps} is in good agreement with the experimental value for the clean Al(100) surface, especially for GGA. The BN and SK schemes give similar results and there is a tendency for the LDA to give a higher Φ_{Ps} than the GGA, opposite to the case for A_+. The negative value of the Ps work function indicates that Ps can be spontaneously emitted from the Al(100) surface. Taking account of the result in Table II, a trapped positron inside a Li-adsorbed Al(100) surface that has a positive work function can combine with a single electron and then be emitted as a Ps atom toward the vacuum.

Table IV shows the Ps^- work functions, Φ_{Ps^-}, for the Al(100) surface with various Li coverage calculated using

$$\begin{aligned}\Phi_{Ps^-} &= 2\Phi_- + \Phi_+ - E_b^{Ps^-} \\ &= -A_+ + \Phi_- - E_b^{Ps^-}, \end{aligned} \qquad (12)$$

where $E_b^{Ps^-} = 7.13$ eV, which is the binding energy for Ps^- (Ref. [62]). For the clean Al(100) surface, Φ_{Ps^-} is calculated to be positive, and the GGA result is in reasonably good agreement with the experimental value, while the LDA gives rather higher values. When the surface is covered with Li atoms, Φ_{Ps^-} shows a strong dependence on the Li coverage; Φ_{Ps^-} is significantly decreased at 0.25 ML coverage and increases again at higher coverage until 1.00 ML. For all calculations, the BN and SK schemes give similar results, and the LDA gives higher Φ_{Ps^-} than GGA. The dependence of Φ_{Ps^-} on the Li coverage can be understood from that of A_+ and Φ_-, as given in Eq. (12). A notable feature of Φ_{Ps^-} is the large negative values at low Li coverage, 0.25–0.50 ML. This is essential for efficient emission of Ps^- from the surface.

TABLE IV. Work functions of Ps^- (Φ_{Ps^-}) for Al(100) surfaces with various Li coverage, calculated with the BN and SK schemes for LDA and GGA and that reported for an experiment (in eV).

	LDA		GGA		
	$\Phi_{Ps^-}^{BN}$	$\Phi_{Ps^-}^{SK}$	$\Phi_{Ps^-}^{BN}$	$\Phi_{Ps^-}^{SK}$	$\Phi_{Ps^-}^{exp}$
Clean	1.60	1.59	1.38	1.36	1.11[a]
Li adsorbed					
0.25 ML	−0.595	−0.611	−0.816	−0.837	–
0.50 ML	−0.308	−0.324	−0.529	−0.550	–
0.75 ML	0.147	0.132	−0.073	−0.093	–
1.00 ML	0.549	0.534	0.329	0.308	–

[a]Ref. [65].

TABLE V. Positron lifetimes (τ) at Al(100) surfaces with various Li coverage, calculated with the BN and SK schemes for LDA and GGA and that for Al bulk and from experimental data (in ps).

	LDA		GGA		
	τ^{BN}	τ^{SK}	τ^{BN}	τ^{SK}	τ^{exp}
Clean	562	507	613	579	580 ± 10[a]
Li adsorbed					
0.25 ML	432	396	455	408	–
0.50 ML	311	295	288	276	–
0.75 ML	263	250	218	217	–
1.00 ML	172	171	175	174	–
Al bulk	163	163	169	170	166[b]

[a]Ref. [68].
[b]Ref. [69].

Therefore, Ps^- can be reemitted from a Li-adsorbed Al(100) surface after positron irradiation. Ps^- has a negative charge and can be accelerated in an electric field; therefore, it is possible to create an energy-tunable Ps beam from Ps^-.

B. Positron surface state

We now present the results for the positron surface state at Li-adsorbed Al(100) surfaces. Table V shows the results for the positron lifetimes τ, for Al(100) surfaces with various Li coverage. We briefly discuss the effect of electron-correlation functionals on τ before consideration of the dependence on coverage. The values of τ calculated with the BN and SK schemes show some differences, which indicates that the calculation of τ is more influenced by the choice of the electron-correlation potential and enhancement factor. For the clean surface, τ^{SK} (GGA) is in good agreement with the experimental value, while τ^{SK}(LDA) shows a large deviation. The differences in these results between the BN and SK schemes become smaller at higher Li coverage, especially at 1.00 ML. This is also the case for the calculation of τ in the Al bulk, in which the calculated results were consistent with the experimental data. Considering the effect of functionals on τ, it would be important to clarify the differences in results obtained with different functionals in a more systematic way. We note that Drummond *et al.* have developed a new local functional based on accurate quantum Monte Carlo calculations [66], which is expected to be the most accurate functional to date [67] and is promising for the comparative study of τ in the future work.

Regarding the dependence of τ on the coverage in Table V, both the LDA and GGA in either the BN or SK scheme indicate a monotonic decrease in τ with increasing Li coverage. In particular, τ at 1.00 ML becomes close to that in the Al bulk. To understand this aspect, the positron effective-potential (V_{eff}^+), calculated as the sum of ϕ' [Eq. (4)] and electron-positron correlation potential, are plotted together with the positron density distribution (n_+) along the z direction in Fig. 2. Side and top views of n_+ in the surface region are presented in Fig. 3. The positron has a positive charge, so that there are repulsive (attractive) interactions between positrons and ions (electrons), which explains the V_{eff}^+ in the interior region of the Al slab in Fig. 2(a). On the other hand, there are significant

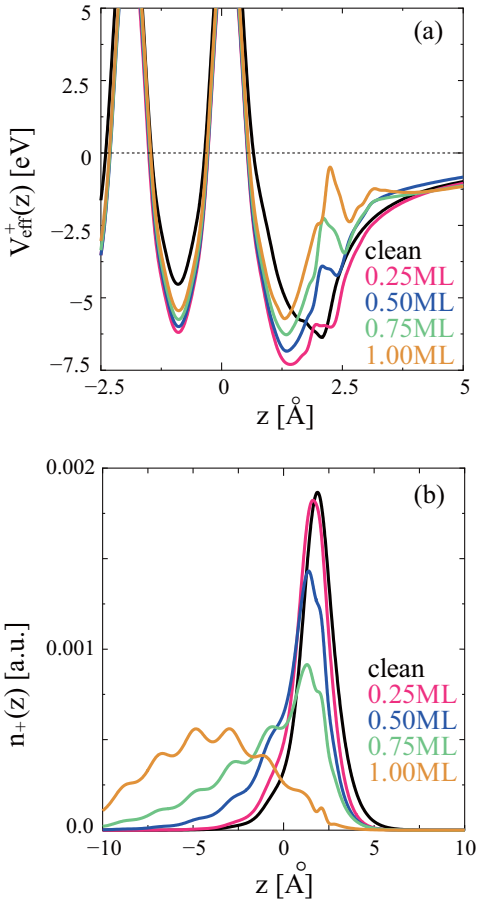

FIG. 2. (Color online) Laterally averaged (a) positron effective potential (V_{eff}^+) and (b) positron density distribution (n_+) along the z direction (perpendicular to the Al(100) surface). $V_{eff}^+ = 0$ is the vacuum level and $z = 0$ is the atomic position of the topmost surface layer. The black, red, blue, green, and orange curves represent $V_{eff}^+(z)$ and $n_+(z)$ for the clean Al(100) surface, and that with 0.25 ML, 0.50 ML, 0.75 ML, and 1.00 ML coverage, respectively.

changes in the V_{eff}^+ with different Li coverage, which indicates that Li adatoms have a significant influence on the positron properties. In Fig. 2(b), there is an apparent shift of the $n_+(z)$ peak positions toward the $-z$ direction (the interior region of the slab) with increasing Li coverage. For the clean surface, the positron is localized in the surface image-potential region. However, when Li atoms are adsorbed, $n_+(z)$ is pushed from the Li adatoms to the Al substrate and broadened. This feature is also clearly evident in Fig. 3 for the Li coverage up to 0.5 ML, where the positron is distributed so as to avoid the Li adatoms. The n_+ over the surface at 0.75 ML becomes low and also distributed to avoid Li adatoms as in the low-coverage case (not shown here). The high electron density in the Al substrate means that a positron can easily annihilate with an electron, which is why τ decreases with increasing Li coverage. It is noted that at 1.00 ML coverage, $n_+(z)$ spreads in the interior region of the slab, as shown in Fig. 2(b). Therefore, τ at 1.00 ML becomes close to that in the Al bulk. These τ characteristics emphasize that τ is highly dependent on the surface electronic states, which are modified by Li adsorption.

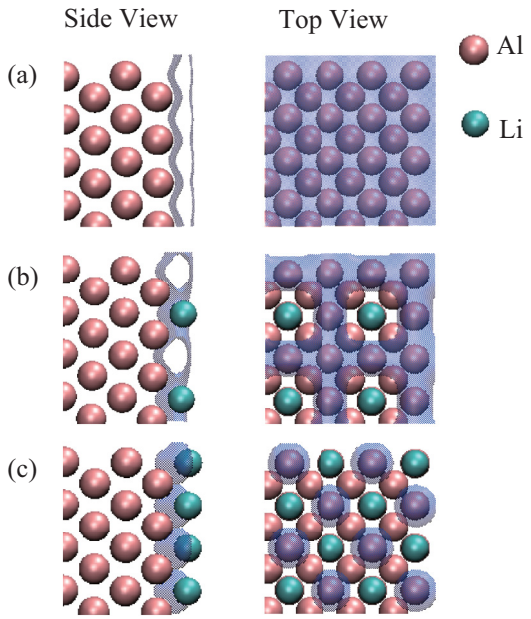

FIG. 3. (Color online) Side and top views of positron density distributions in Al(100) surfaces with various Li coverage; (a) clean, (b) 0.25 ML, and (c) 0.50 ML. The positron density is shown as a blue transparent isosurface with an isovalue of 0.0015 a.u. The Al and Li atoms are represented by light brown and cyan colored balls, respectively.

Table VI shows the positron binding energy (E_b), which is calculated as the difference between the vacuum level and the Fermi energy of the positron that is trapped by the surface-induced image potential. The E_b values calculated from both LDA and GGA are in good agreement with the experimental data for the clean Al(100) surface. E_b increases with Li adsorption at 0.25 ML and decreases with increasing Li coverage. The dependence of E_b on the Li coverage is similar to that for the positron work function given in Table II, which is due to the change in the surface dipole barrier. This can be interpreted from Fig. 2(a); the positron effective potential has a well near the effective image plane ($z_0 = 1.63$ Å for the clean surface), where the well depth is the largest at 0.25 ML coverage and then decreases with

TABLE VI. Positron binding energies (E_b) for Al(100) surfaces with various Li coverage, calculated with the BN and SK schemes for the LDA and GGA and that reported for experiments (in eV).

	LDA		GGA		
	E_b^{BN}	E_b^{SK}	E_b^{BN}	E_b^{SK}	E_b^{exp}
Clean	3.08	3.10	2.89	2.89	3.03[a], 2.80[b]
Li adsorbed					
0.25 ML	4.54	4.51	4.29	4.31	–
0.50 ML	4.11	4.07	3.92	3.90	–
0.75 ML	3.39	3.36	3.29	3.24	–
1.00 ML	3.00	2.97	2.96	2.93	–

[a]Ref. [70].
[b]Ref. [71].

TABLE VII. Activation energies E_a of thermalized Ps for Al(100) surfaces with various Li coverage, calculated with the BN and SK schemes for LDA and GGA and that reported from experiments (in eV).

	LDA		GGA		
	E_a^{BN}	E_a^{SK}	E_a^{BN}	E_a^{SK}	E_a^{exp}
Clean	0.67	0.69	0.49	0.49	0.64[a], 0.49[b]
Li adsorbed					
0.25 ML	−0.07	−0.09	−0.31	−0.29	–
0.50 ML	−0.20	−0.24	−0.40	−0.42	–
0.75 ML	−0.47	−0.50	−0.57	−0.62	–
1.00 ML	−0.45	−0.49	−0.50	−0.53	–

[a]Ref. [72].
[b]Ref. [73].

increasing Li coverage, having a tendency similar to that for E_b. Accordingly, the dependence of E_b on the Li coverage is attributed to the rearrangement of the surface-electron charge distribution caused by electron transfer from the Li adatoms to the Al substrate.

Based on these results for E_b, the activation energy E_a for the positron trapped by the image potential, which becomes a thermalized Ps atom and is then emitted toward the vacuum, is given in Table VII. E_a is calculated from [71]

$$E_a = E_b + \Phi_- - E_b^{Ps}. \quad (13)$$

For the clean Al(100) surface, the calculated E_a is positive and overall the LDA and GGA results agree with the experimental values. This agreement is not trivial. It was shown in the previous study by Cuthbert that the E_a for the Al clean surface is negative in the hydrodynamic model with the consideration of the interaction of a positron with the electron gas (the positron channel), while the E_a becomes positive if considering the interaction of the electron gas with the electron-positron composite (the Ps channel) [74]. The work of Cuthbert has been confirmed by Platzman and Tzoar [75]. Furthermore, the Ps channel has been recently considered within robust formalism based on electronic ground-state DFT calculation and applied to study Ps surface states in quartz [76] and in topological insulators [77]. In our TC-DFT simulation, electrons and a positron are treated on an equal footing, and it relies on the exchange-correlation functional to give correct electron-positron interaction. The fact that our result of the Al clean surface agrees with those of previous Ps channel calculations indicates the effectiveness of the present TC-DFT implementation.

When Li atoms are adsorbed, E_a in Table VII becomes negative and decreases as the Li coverage increases from 0.25 to 0.75 ML. The E_a shows a maximum magnitude at a coverage of 0.75 ML; this dependence of E_a on the coverage is not a general property for adsorbed surfaces but rather specific to Li-adsorbed Al(100) surface. In fact, dependence of E_a on the coverage was found to be different with respect to the adsorbed surfaces in the previous study [78,79]. The feature is due to the fact that E_a is determined by two factors, E_b and Φ_-, which have different dependence on the coverage. The results of Table VII, together with those in Tables II and III,

indicate that if a low-energy positron is injected to the Al(100) surface covered with Li adatoms, then the positron can go back from the bulk to the surface, combine with a single electron to become a Ps atom, and then be emitted toward the vacuum. Following these results and discussions, we predict that Ps emission from the Al(100) surface is considerably enhanced with increasing Li adsorption.

V. CONCLUSIONS

The positron surface state and the energetics for positron reemission process from Al(100) surfaces with various lithium atom coverage were investigated using TC-DFT in the PAW framework. The self-consistent electronic structures of fully relaxed atomic geometries obtained from slab calculations were used as the input for the positron calculations. With implementation of the surface image potential and the ramp potential, the TC-DFT simulation has given good results both for the positron affinity and the electronic work functions, from which positron, Ps, and Ps^- work functions were directly calculated. These results agree fairly well with the experimental data for the clean Al(100) surface.

For the surfaces covered with Li adatoms, the calculated results indicate a strong dependence of the work functions for electrons, positrons, and Ps^- on the coverage, which can be understood from analysis of the surface dipole barrier. In particular, the Ps^- work function is significantly reduced at low Li-coverage, and becomes negative, similar to that for Ps. Therefore, injected positrons can be reemitted as Ps^- together with Ps. In addition, Ps^- has a negative charge and can be accelerated in an electric field; therefore, it is possible to generate an energy-tunable Ps beam from Ps^-. Furthermore, the calculations well reproduced the positron surface-state lifetime for a clean Al(100) surface, as well as the experimentally observed positron binding energy and activation energy. The positron lifetime is determined as a decreasing function of the Li coverage and the activation energy of Ps is significantly reduced at certain Li coverage, which leads to an abrupt increase in Ps reemission from such Li-adsorbed Al(100) surfaces.

ACKNOWLEDGMENTS

The authors thank Y. Nagashima for valuable comments and information of experiments on surface positrons. Parallelized calculations were performed on the supercomputers of the Institute for Solid State Physics, The University of Tokyo.

[1] M. J. Puska and R. Nieminen, Rev. Mod. Phys. **66**, 841 (1994).
[2] F. Tuomisto and I. Makkonen, Rev. Mod. Phys. **85**, 1583 (2013).
[3] A. Dupasquier and A. Mills, Jr., *Positron Spectroscopy of Solids*, Vol. 125 (IOS Press, Amsterdam, 1995).
[4] D. A. Fischer, K. G. Lynn, and W. E. Frieze, Phys. Rev. Lett. **50**, 1149 (1983).
[5] A. Weiss, R. Mayer, M. Jibaly, C. Lei, D. Mehl, and K. G. Lynn, Phys. Rev. Lett. **61**, 2245 (1988).
[6] T. Tachibana, T. Hirayama, and Y. Nagashima, Phys. Rev. B **89**, 201409 (2014).
[7] Y. Fukaya, I. Mochizuki, M. Maekawa, K. Wada, T. Hyodo, I. Matsuda, and A. Kawasuso, Phys. Rev. B **88**, 205413 (2013).
[8] K. Michishio, T. Tachibana, R. Suzuki, K. Wada, A. Yagishita, T. Hyodo, and Y. Nagashima, Appl. Phys. Lett. **100**, 254102 (2012).
[9] Y. Nagashima, Phys. Rep. **545**, 95 (2014).
[10] K. Michishio, T. Tachibana, H. Terabe, A. Igarashi, K. Wada, T. Kuga, A. Yagishita, T. Hyodo, and Y. Nagashima, Phys. Rev. Lett. **106**, 153401 (2011).
[11] C. Hodges and M. Stott, Solid State Commun. **12**, 1153 (1973).
[12] R. Nieminen and M. Manninen, Solid State Commun. **15**, 403 (1974).
[13] M. Puska and R. Nieminen, J. Phys. F **13**, 333 (1983).
[14] R. M. Nieminen and K. O. Jensen, Phys. Rev. B **38**, 5764 (1988).
[15] K. O. Jensen and A. Weiss, Phys. Rev. B **41**, 3928 (1990).
[16] N. G. Fazleev, J. L. Fry, K. H. Kuttler, A. R. Koymen, and A. H. Weiss, Phys. Rev. B **52**, 5351 (1995).
[17] N. G. Fazleev, J. L. Fry, and A. H. Weiss, Phys. Rev. B **70**, 165309 (2004).
[18] N. Fazleev, Appl. Surf. Sci. **252**, 3333 (2006).
[19] B. Chakraborty, Phys. Rev. B **24**, 7423 (1981).
[20] E. Boroński and R. M. Nieminen, Phys. Rev. B **34**, 3820 (1986).
[21] M. J. Puska, S. Mäkinen, M. Manninen, and R. M. Nieminen, Phys. Rev. B **39**, 7666 (1989).
[22] M. Puska, J. Phys.: Condens. Matter **3**, 3455 (1991).
[23] M. Saito, A. Oshiyama, and S. Tanigawa, Phys. Rev. B **44**, 10601 (1991).
[24] A. Nakamoto, M. Saito, T. Yamasaki, M. Okamoto, T. Hamada, and T. Ohno, Jpn. J. Appl. Phys. **47**, 2213 (2008).
[25] A. Kawasuso, M. Maekawa, Y. Fukaya, A. Yabuuchi, and I. Mochizuki, Phys. Rev. B **83**, 100406 (2011).
[26] A. Kawasuso, M. Maekawa, Y. Fukaya, A. Yabuuchi, and I. Mochizuki, Phys. Rev. B **85**, 024417 (2012).
[27] J. Wiktor, G. Jomard, M. Torrent, and M. Bertolus, Phys. Rev. B **87**, 235207 (2013).
[28] J. Lin, T. Yamasaki, and M. Saito, Jpn. J. Appl. Phys. **53**, 053002 (2014).
[29] L. Gilgien, G. Galli, F. Gygi, and R. Car, Phys. Rev. Lett. **72**, 3214 (1994).
[30] M. J. Puska, A. P. Seitsonen, and R. M. Nieminen, Phys. Rev. B **52**, 10947 (1995).
[31] M. Saito and A. Oshiyama, Phys. Rev. B **53**, 7810 (1996).
[32] Y. Nagai, Z. Tang, M. Hassegawa, T. Kanai, and M. Saneyasu, Phys. Rev. B **63**, 134110 (2001).
[33] D. V. Makhov and L. J. Lewis, Phys. Rev. B **71**, 205215 (2005).
[34] A. Kawasuso, M. Yoshikawa, H. Itoh, T. Chiba, T. Higuchi, K. Betsuyaku, F. Redmann, and R. Krause-Rehberg, Phys. Rev. B **72**, 045204 (2005).
[35] Z. Q. Chen, K. Betsuyaku, and A. Kawasuso, Phys. Rev. B **77**, 113204 (2008).
[36] M. Maekawa and A. Kawasuso, Jpn. J. Appl. Phys. **48**, 030203 (2009).
[37] J. Wiktor, X. Kerbiriou, G. Jomard, S. Esnouf, M.-F. Barthe, and M. Bertolus, Phys. Rev. B **89**, 155203 (2014).

[38] K. Jensen and A. Walker, J. Phys. F **18**, L277 (1988).
[39] A. Rubaszek and J. Lach, J. Phys.: Condens. Matter **1**, 9243 (1989).
[40] A. Rubaszek, Phys. Rev. B **44**, 10857 (1991).
[41] R. M. Nieminen, E. Boronski, and L. J. Lantto, Phys. Rev. B **32**, 1377 (1985).
[42] R. M. Nieminen and M. J. Puska, Phys. Rev. Lett. **50**, 281 (1983).
[43] N. Lang and W. Kohn, Phys. Rev. B **7**, 3541 (1973).
[44] C. Hodges and M. Stott, Phys. Rev. B **7**, 73 (1973).
[45] R. M. Nieminen and J. Oliva, Phys. Rev. B **22**, 2226 (1980).
[46] O. V. Boev, M. J. Puska, and R. M. Nieminen, Phys. Rev. B **36**, 7786 (1987).
[47] M. Puska, P. Lanki, and R. Nieminen, J. Phys.: Condens. Matter **1**, 6081 (1989).
[48] R. M. Nieminen, M. J. Puska, and M. Manninen, Phys. Rev. Lett. **53**, 1298 (1984).
[49] X. Gonze *et al.*, Comput. Mater. Sci. **25**, 478 (2002).
[50] X. Gonze *et al.*, Comput. Phys. Commun. **180**, 2582 (2009).
[51] P. E. Blöchl, Phys. Rev. B **50**, 17953 (1994).
[52] M. Torrent, F. Jollet, F. Bottin, G. Zérah, and X. Gonze, Comput. Mater. Sci. **42**, 337 (2008).
[53] N. Holzwarth, A. Tackett, and G. Matthews, Comput. Phys. Commun. **135**, 329 (2001).
[54] J. P. Perdew, K. Burke, and M. Ernzerhof, Phys. Rev. Lett. **77**, 3865 (1996).
[55] J. Arponen and E. Pajanne, Ann. Phys. **121**, 343 (1979).
[56] P. A. Sterne and J. H. Kaiser, Phys. Rev. B **43**, 13892 (1991).
[57] B. Barbiellini, M. J. Puska, T. Torsti, and R. M. Nieminen, Phys. Rev. B **51**, 7341 (1995).
[58] B. Barbiellini, M. J. Puska, T. Korhonen, A. Harju, T. Torsti, and R. M. Nieminen, Phys. Rev. B **53**, 16201 (1996).
[59] J. Kuriplach and B. Barbiellini, Phys. Rev. B **89**, 155111 (2014).
[60] A. P. Mills, Jr., L. Pfeiffer, and P. M. Platzman, Phys. Rev. Lett. **51**, 1085 (1983).
[61] C. A. Murray, A. P. Mills, Jr., and J. Rowe, Surf. Sci. **100**, 647 (1980).
[62] Y. Nagashima, T. Hakodate, A. Miyamoto, and K. Michishio, New J. Phys. **10**, 123029 (2008).
[63] J. Grepstad, P. Gartland, and B. Slagsvold, Surf. Sci. **57**, 348 (1976).
[64] C. A. Murray and A. P. Mills, Jr., Solid State Commun. **34**, 789 (1980).
[65] Y. Nagashima, T. Hakodate, and T. Sakai, Appl. Surf. Sci. **255**, 217 (2008).
[66] N. D. Drummond, P. López Ríos, R. J. Needs, and C. J. Pickard, Phys. Rev. Lett. **107**, 207402 (2011).
[67] W. Zhang, J. Liu, J. Zhang, S. Huang, J. Li, and B. Ye, JJAP Conf. Proc. **2**, 011001 (2014).
[68] K. G. Lynn, W. E. Frieze, and P. J. Schultz, Phys. Rev. Lett. **52**, 1137 (1984).
[69] M. J. Fluss, L. C. Smedskjaer, M. K. Chason, D. G. Legnini, and R. W. Siegel, Phys. Rev. B **17**, 3444 (1978).
[70] A. P. Mills, Jr., Solid State Commun. **31**, 623 (1979).
[71] P. J. Schultz and K. G. Lynn, Rev. Mod. Phys. **60**, 701 (1988).
[72] I. Rosenberg, A. Weiss, and K. Canter, J. Vac. Sci. Tech. **17**, 253 (1980).
[73] K. Lynn, Phys. Rev. Lett. **44**, 1330 (1980).
[74] A. Cuthbert, J. Phys. C **18**, 4561 (1985).
[75] P. M. Platzman and N. Tzoar, Phys. Rev. B **33**, 5900 (1986).
[76] R. Saniz, B. Barbiellini, P. M. Platzman, and A. J. Freeman, Phys. Rev. Lett. **99**, 096101 (2007).
[77] R. Saniz, S. Vercauteren, D. Lamoen, B. Partoens, and B. Barbiellini, J. Phys.: Conf. Ser. **505**, 012002 (2014).
[78] D. W. Gidley, A. R. Köymen, and T. W. Capehart, Phys. Rev. B **37**, 2465 (1988).
[79] S. Chu, A. P. Mills, Jr., and C. A. Murray, Phys. Rev. B **23**, 2060 (1981).